LETTER Communicated by John Milton

Multistability in Spiking Neuron Models of Delayed Recurrent Inhibitory Loops

Jianfu Ma
majianfu@mathstat.yorku.ca
Jianhong Wu
wujh@mathstat.yorku.ca
Laboratory for Industrial and Applied Mathematics, Department of Mathematics and Statistics, York University, Toronto, Ontario M3J 1P3, Canada

We consider the effect of the effective timing of a delayed feedback on the excitatory neuron in a recurrent inhibitory loop, when biological realities of firing and absolute refractory period are incorporated into a phenomenological spiking linear or quadratic integrate-and-fire neuron model. We show that such models are capable of generating a large number of asymptotically stable periodic solutions with predictable patterns of oscillations. We observe that the number of fixed points of the so-called phase resetting map coincides with the number of distinct periods of all stable periodic solutions rather than the number of stable patterns. We demonstrate how configurational information corresponding to these distinct periods can be explored to calculate and predict the number of stable patterns.

1 Introduction

In a living nervous system, recurrent loops involving two or more neurons are ubiquitous and are particularly prevalent in cortical regions for memory such as the hippocampal-mesial temporal lobe complex (Traub & Miles, 1991). The simplest recurrent inhibitory loop (see Figure 1) in a neural network consists of an excitatory neuron E and an inhibitory neuron I, where neuron E gives off collateral branches and excites the inhibitory neuron I, which in turns inhibits the firing of E, in a delay time. (See Foss, Longtin, Mensour, & Milton, 1996; Mackey & an der Heiden, 1984; Mackey & Milton, 1987.) These previous studies show that two-neuron inhibitory loops with delay display similar complex dynamic behaviors as larger networks such as multistability, and many techniques developed to deal with two-neuron networks can carry over to large-size networks. Therefore, the two-neuron recurrent inhibitory loops have been used as prototypes to improve our understanding of the impact on the network's computational performance of the interaction of time delay and inhibitory feedback.

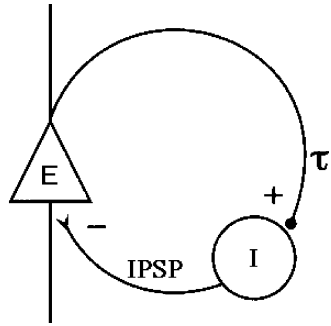

Figure 1: A recurrent neuron loop consists of an excitatory neuron E and an inhibitory neuron I, where neuron E excites the neuron I, which delivers an inhibitory postsynaptic potential (IPSP) to the neuron E, in a time lag τ.

An interesting computational behavior of a delayed inhibitory loop is multistability: the coexistence of multiple stable patterns such as equilibria and periodic orbits. The coexistence of multiple equilibria in a neural network is the basis of the mechanism for (associative) content-addressable memory and retrieval (Foss et al., 1996; Hopfield, 1982, 1984; Milton, 2000; Morita, 1993) where each equilibrium is identified with static memory, while stable periodic orbits are associated with temporally patterned spike trains (Canavier, Baxter, Clark, & Byrne, 1994; Foss et al., 1996; Foss, Moss, & Milton, 1997). Multistability in a delayed neural network has been extensively studied in the literature, in particular for delayed neural recurrent loops (Foss et al., 1996, 1997), and experimentally in electrical circuits (Foss et al., 1997) and recurrently clamped neurons (Foss & Milton, 2000). The rigorous mathematical investigation of the coexistence of multiple periodic orbits and the description of the domains of attraction of periodic solutions as well as the structure of the global attractor can be found in Chen and Wu (1999, 2000, 2001a, 2001b, 2001c) and Chen, Wu, and Krisztin (2000).

Time delays, a powerful mechanism for multistability, are intrinsic properties of the nervous systems and are unavoidable in electronic implementation due to axonal conduction times, distances of interneurons, and the finite switching speeds of amplifiers. An essential requirement for delay-induced multistability in a delayed feedback loop is that the delay must be longer than the response time of the system or intrinsic period of the spiking neuron (Foss et al., 1996, 1997; Ikeda & Matsumoto, 1987). An example is the delay differential equation,

$$\frac{dx(t)}{dt} = -\alpha x(t) + F(x(t-\tau)), \tag{1.1}$$

where α is a positive constant and F is the feedback function. The work of an der Heiden and Mackey (1992) and Ikeda and Matsumoto (1987) suggested that multistability occurs when the time delay τ is longer than the intrinsic timescale of the control mechanism, i.e., $\tau > \alpha^{-1}$, and the feedback function F is nonmonotonic. Losson (1991) and Losson, Mackey, and Longtin (1993) studied equation 1.1 with the feedback function

$$F(x) = \begin{cases} c & \text{if } x \in [x_1, x_2]; \\ 0 & \text{otherwise } (x < x_1 \text{ or } x > x_2), \end{cases} \tag{1.2}$$

and observed three coexisting attracting nonconstant periodic solutions when $\alpha = 3.25$, $c = 20.5$, $x_1 = 1$, $x_2 = 2$, and $\tau = 1$. The Mackey-Glass delay differential equation (Mackey & Glass, 1997), given by

$$\frac{dx(t)}{dt} = -\alpha x(t) + \frac{\beta x(t-1)}{1 + x(t-1)^{10}}, \tag{1.3}$$

and originally introduced to model oscillations in neutrophil populations, was found to have four coexisting, attracting periodic solutions in symmetric positive and negative pairs. Furthermore, Foss et al. (1996) studied neural recurrent inhibitory loops using the well-known Hodgkin-Huxley model (see details below) and found three coexisting attracting periodic solutions.

Another important concept related to multistability is the phase resetting curve (PRC), which describes the phase shift of an oscillation in response to a perturbation in the neuron's spike times. PRC is a powerful tool to study the effects of perturbations on biological periodic oscillations. Various mathematical models based on phase-resetting properties have been extensively used to study the effect of periodic inhibitory stimulation of cortical slices (Schindler, Bernasconi, Stoop, Goodman, & Douglas, 1997) and the occurrence of multistability in ring circuit models for CPGs (Canavier et al., 1999), and to explain complex dynamical behaviors of large populations of neurons (Hoppensteadt & Izhikevich, 1997). In particular, Foss and Milton (2000) developed a mathematical model that incorporates two measurable parameters involving time delay and phase resetting to investigate the occurrence of multistability in the delayed recurrent loop, where they used multiple fixed points in a phase-resetting map to predict the number of coexistent stable patterns.

Most of this work on inhibitory loops and feedbacks has been based on the consideration of the dynamical behaviors of the single excitatory neuron in the two-neuron inhibitory loop, and hence the model equation takes the form of a scalar delay differential equation that can also arise in modeling of a single neuron with delayed self-feedback. Many of the results require the signal function to be nonmonotone. There are also two popular models

for a single neuron in theoretical neuroscience: phenomenological spiking neuron models and detailed conductance-based neuron models. In comparison with simple phenomenological spiking neuron models, detailed conductance-based neuron models have a high degree of accuracy to measure the intrinsic complexity of a single neuron, such as firing and inhibitory rebound spikes. A well-known example of the detailed conduction-based models is the following Hodgkin-Huxley differential equation:

$$\begin{aligned} Cx'(t) &= I_{ion}(x, m, n, h) + I_{syn}(t) + I_s(t), \\ I_{ion} &= -g_{Na}m^3h(x(t) - E_{Na}) - g_K n^4(x(t) - E_k) - g_L(x(t) - E_L), \end{aligned} \tag{1.4}$$

where $x(t)$ is the membrane potential of the neuron under consideration at time t, C is the membrane capacitance, and I_{ion} is the sum of currents through sodium ion channel, potassium ion channel, and leakage channel. The applied currents have two parts: postsynaptic current I_{syn} (PSC) and external stimulus I_s. Constants g_{Na} and g_K are the maximum conductance of sodium and potassium ion channels, the constant g_L is the conductance of leakage channel, and constants E_{Na}, E_K, and E_L are empirical parameters called the reversal potential. Parameters commonly used are $C = 1$, $g_{Na} = 120$, $g_K = 36$, $g_L = 0.3$, $E_{Na} = 115$, $E_K = -12$, and $E_L = 10.613$. There are three (gating) variables (m, n, h) that describe the probability that a certain channel is open, and these variables evolve according to the following differential equations:

$$\begin{cases} m'(t) = \alpha_m(x)(1 - m) - \beta_m(x)m, \\ n'(t) = \alpha_n(x)(1 - n) - \beta_n(x)n, \\ h'(t) = \alpha_h(x)(1 - h) - \beta_h(x)h, \end{cases} \tag{1.5}$$

where the functions α and β indexed by (m, n, h) are given by

$$\begin{cases} \alpha_n = \frac{0.1-0.01x}{\exp(1-0.1x)-1}, & \beta_n = \frac{0.125}{\exp(x/80)} \\ \alpha_m = \frac{2.5-0.1x}{\exp(2.5-0.1x)-1}, & \beta_m = \frac{4}{\exp(x/18)} \\ \alpha_h = \frac{0.07}{\exp(x/20)}, & \beta_h = \frac{1}{\exp(3-0.1x)+1}. \end{cases} \tag{1.6}$$

Unfortunately, the intrinsic complexity of the conductance-based model makes it difficult for a careful theoretical and qualitative analysis. Thus, simple phenomenological spiking neuron models are introduced especially for the study of neural coding, memory, and network dynamics, in addition to facilitation of engineering implementation. A widely used such model

is the following linear integrate-and-fire model (LIF) for the membrane potential,

$$\frac{dx(t)}{dt} = -\beta x(t) + I_{syn} + I_s(t), \tag{1.7}$$

with the reset condition $\lim_{t \to t_f^+} x(t) = V_r$, where β is the decay rate, V_r is the reset potential, and the firing time t_f is defined by a threshold criterion,

$$t_f : x(t) = \vartheta_1 \quad \text{and} \quad x'(t)|_{t=t_f} > 0, \tag{1.8}$$

with ϑ_1 being the firing threshold. Such a model can be seen as a reduced neural model with a mean excitatory and inhibitory membrane potential (averaged over the neuron). A nonlinear analog is the following quadratic integrate-and-fire model (QIF), given by

$$\begin{aligned} &\frac{dx(t)}{dt} = \beta(x-\mu)(x-\gamma) + I_{syn} + I_s(t) \\ &t_f : x(t) = \vartheta_1 \quad \text{and} \quad x'(t)|_{t=t_f} > 0, \end{aligned} \tag{1.9}$$

with the reset condition $\lim_{t \to t_f^+} x(t) = V_r$, where β is a constant, μ is the critical reversal potential of resting state or inhibitory rebound, and γ is the critical reversal potential of firing. (See Feng, 2001; Hansel & Mato, 2001; Latham, Richmond, Nelson, & Nirenberg, 2000; and discussions below.)

However, simple phenomenological models alone are unable to capture some important biological features exhibited by the detailed conduction-based models, such as the absolute refractory period, which seems to be an important factor for the occurrence of a large number of stable patterns, and as the inhibitory rebound that enables spikes in initial functions to propagate in future time.

This letter analyzes effects of these biological features on multistability in phenomenological models in order to provide effective mechanisms for phenomenological models to generate a huge number of coexisting stable periodic solutions. The core to these mechanisms is the interaction of time lag, inhibitory feedback, firing, rebound, and absolute refractory period, incorporated in a (QIF) model with delayed feedback.

The relative simplicity of the phenomenological QIF model enables us to formulate analytically the relevant phase-resetting map, based on which we find that the number of fixed points of the phase-resetting map coincides exactly with the number of distinct periods of stable periodic solutions rather than with the number of distinct stable patterns. However, using the configurational information corresponding to these distinct periods, we can calculate the number of distinct periodic solutions and precisely predict their patterns.

Basic frameworks of the QIF models with delayed feedback are discussed in section 2, and detailed discussions about QIF models are given in section 3, along with the description of numerical simulations and the connections with phase-resetting techniques. Further comments are presented in the final section.

2 Recurrent Inhibitory Loops: Model Formulation

A recurrent inhibitory loop is composed of two neurons: an excitatory neuron E and an inhibitory neuron I. Injecting a large enough stimulus I_s into the dendrite of the neuron E causes its membrane potential to increase until it reaches its firing threshold ϑ_1. The neuron E fires and emits an action potential or spike, and then the membrane potential is reset to a certain value V_r (called *reset membrane potential*). In the absence of stimulus, a single neuron is at rest, and the corresponding membrane potential is called the *resting membrane potential* V_0. The perpetuated stimulus causes the neuron to emit a sequence of spikes called a *spike train*. In the absence of recurrent inhibition, the period of spikes in the spike train is called the *intrinsic spiking period* of the excitatory neuron E, denoted by T in the remaining part of this article. The firing of neuron E excites the inhibitory interneuron I, which delivers an inhibitory postsynaptic potential (IPSP) to the excitatory neuron E.

Foss et al. (1996) described the membrane potential of the excitatory neuron E using the Hodgkin-Huxley model (HH) by considering the effect of IPSP as self-feedback. They obtained the following delay differential system,

$$\begin{cases} Cx'(t) = -g_{Na}m^3h(x(t)-E_{Na}) - g_K n^4(x(t)-E_k) - g_L(x(t)-E_L) \\ \qquad\qquad -F(x(t-\tau)) + I_s(t), \\ m'(t) = \alpha_m(x)(1-m) - \beta_m(x)m, \\ n'(t) = \alpha_n(x)(1-n) - \beta_n(x)n, \\ h'(t) = \alpha_h(x)(1-h) - \beta_h(x)h, \end{cases} \tag{2.1}$$

where $F(x)$ is the signal function that describes the effect of the inhibitory neuron I on the membrane potential of the excitatory neuron E, and τ is the time lag. The corresponding linear integrate-and-fire model (LIF) and quadratic integrate-and-fire model (QIF) are given by

$$x'(t) = -\beta x(t) - F(x(t-\tau)) + I_s(t), \tag{2.2}$$

$$x'(t) = \beta(x-\mu)(x-\gamma) - F(x(t-\tau)) + I_s(t), \tag{2.3}$$

with firing time t_f,

$$t_f : x(t) = \vartheta_1 \quad \text{and} \quad x'(t)|_{t=t_f} > 0,$$

and firing threshold ϑ_1.

In order to specify a solution of the above delay differential equations, it is necessary to give an initial function ϕ in the interval $[-\tau, 0]$. In what follows, the initial function has the form of neural spike trains. Namely, it is given by a sum of square pulse functions as follows:

$$\phi(t) = \sum \psi(t - t_i), \tag{2.4}$$

where

$$\psi(t) = \begin{cases} c & \text{if } t \in [0, d]; \\ 0 & \text{otherwise,} \end{cases} \tag{2.5}$$

with c being the amplitude of the action potential (e.g., $c = 100$ mV in the Hodgkin-Huxley model) and d the duration of a spike. We shall use the following piecewise nondecreasing constant function,

$$F_1(x) = \begin{cases} a & \text{if } x \geq \vartheta_1; \\ 0 & \text{otherwise,} \end{cases} \tag{2.6}$$

where a is a positive constant. For simplification, we set the resting membrane potential to zero ($V_0 = 0$).

3 Simulations and Analysis

In what follows, we address the multistability issue in two regions classified by the nature of the stimulus I_s: the excitable regime where I_s cannot make the neuron fire and the periodic regime where I_s makes the neuron fire successively.

3.1 Hodgkin-Huxley Model (HH). When $\tau = 116$ msec and the signal function $F(x) = \mu x$ with a constant μ, Foss et al. (1996) found that in the excitable region $I_s = 0$, each initial function ϕ gives rise to a solution that is eventually periodic. These eventually periodic solutions are stable, but the model has no coexisting attractor. In the periodic regime $I_s = 10$ μA, however, they found three coexisting attracting periodic solutions.

We obtained similar results using the piecewise constant function $F(x) = F_1(x)$. In particular, for the piecewise constant function and in the excitable regime $I_s = 0$, we found that different initial functions give rise to different, eventually periodic, solutions that are stable and there is no

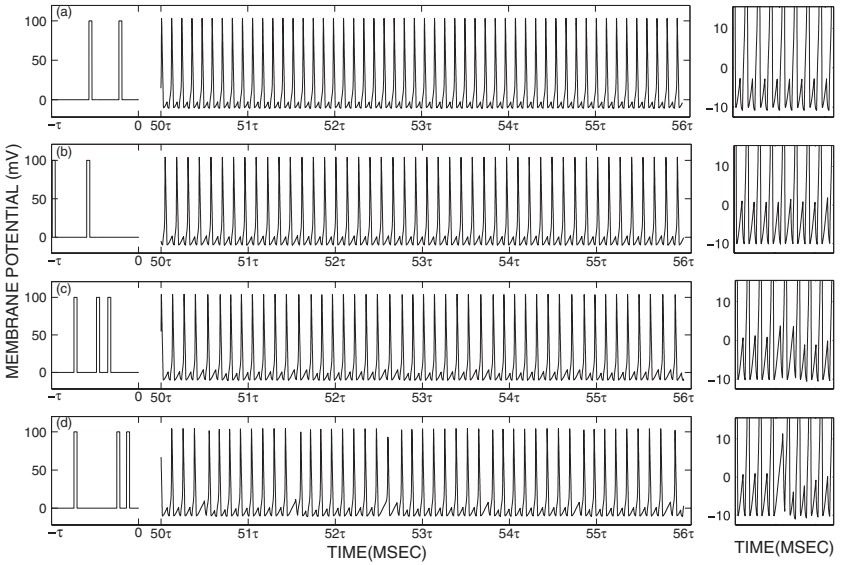

Figure 2: Four coexisting attracting periodic solutions generated by the excitatory neuron E for the Hodgkin-Huxley model (HH) given by equations 2.1 with the piecewise constant signal function $F_1(x)$ when $I = 10\,\mu$A, $\tau = 116$ msec, $\vartheta_1 = 18.6$ mV, and $a = 16$. Spikes in the initial function ϕ on the interval $(-\tau, 0)$ are 4 msec in duration. After 50τ of transients, the periodic solutions are output in six delay intervals. The right-hand side is the blow-up of the solutions in a given period (not delay τ) to clearly illustrate the patterns of solutions.

coexisting attractor. But in the periodic regime $I_s = 10\ \mu$A with parameters $\tau = 116$ msec, $\vartheta_1 = 18.6$ mV, and $a = 16$, we found four coexisting periodic attractors shown in Figure 2. The corresponding trajectories exhibit exotic transient behaviors but eventually become periodic.

3.2 LIF Model with Firing and Absolute Refractoriness. Each time the excitatory neuron fires a spike, a feedback is delivered at time τ later. Since the exact time course of action potential carries no information, for most of our study of the simple phenomenological spiking neuron models, the form of action potential may be neglected and the action potential is characterized by firing time t_f and the reset condition. For our linear and quadratic integrate-and-fire models, the type of multistability not only depends on the time delay τ but also on the effective timing of the feedback that affects the excitatory neuron. The total timing of the feedback, denoted by T_ϑ, is the portion of the duration when the spike is above the firing threshold. This total timing of the feedback is not characterized by the reset condition and firing time mentioned in the simple phenomenological

spiking neuron models. To simplify our presentation and simulations, we now introduce an approximation of the spike time course.

3.3 Firing. If the membrane potential reaches its firing threshold ϑ_1 from below at a moment t_f, an action potential (spike) is generated, and then the membrane potential is reset to the reset potential $V_r < 0$. As the shapes of spikes vary little and the form of an action potential is insignificant to the LIF model, we can represent the time course of the membrane potential by any function that increases from ϑ_1 to c first and then decreases to V_r. In our work, we choose the following continuous linear function,

$$x_f(t) = \hat{x}_1(t) = \begin{cases} \vartheta_1 + \frac{c-\vartheta_1}{s_1-t_f}(t-t_f) & \text{if } t \in [t_f, s_1) \\ V_r + \frac{c-V_r}{s_2-s_1}(s_2-t) & \text{if } t \in [s_1, s_2], \end{cases} \tag{3.1}$$

or the continuous exponential function,

$$x_f(t) = \hat{x}_2(t) = \begin{cases} \vartheta_1 e^{\alpha_1(t-t_f)} & \text{if } t \in [t_f, s_1] \\ e^{-\alpha_2(s_2-t)}\left[\frac{V_r}{s_2-s_1}(t-s_1) + \frac{c\,e^{\alpha_2(s_2-s_1)}}{s_2-s_1}(s_2-t)\right] & \text{if } t \in (s_1, s_2], \end{cases} \tag{3.2}$$

where c is the amplitude of action potential and $s_1 < s_2$ are the times when $x(t) = c$ and $x(t) = V_r$, respectively. All simulation results reported below are based on the function $\hat{x}_1$. To simplify our simulation, we take $c = 10\,\text{mV}$ for the rest of this article. We emphasize again that we introduce explicitly the firing time course of the membrane potential in order to have the continuity for the action potential; all that is really needed for the analysis and simulations is the timing for firing and the three parameters ϑ_1, c, and V_r.

3.4 Absolute Refractory Period. The second factor determining the effective timing of the feedback is the absolute refractory period, a short period after the firing of a spike during which the neuron is not affected by inputs at all. Without the input term $I(t) = I_s(t) - F(x(t-\tau))$, equation 2.2 becomes

$$\frac{dx}{dt} = -\beta x, \tag{3.3}$$

with the corresponding solution given by

$$x_{abs}(t) = V_r e^{-\beta(t-s_2)}, \tag{3.4}$$

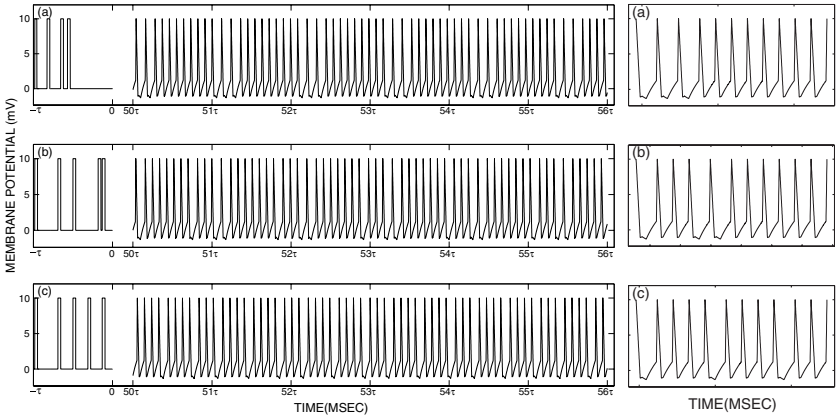

Figure 3: Three coexisting attracting periodic solutions (patterns 3w8v, 1w2v2w6v, 1w3v1w3v1w2v) generated by the LIF model given by equation 2.2 with the signal function $F_1(x)$ for $I_s = 0.38\,\mu$A. Parameters are $\tau = 116$ msec, $\beta = 0.08$, $c = 10$ mV, $a = 0.6$, $s_1 - t_f = 0.60$ msec, $s_2 - s_1 = 2.7$ msec, $\vartheta_1 = 1.2$ mV, $V_r = -1.1$ mV, and $d_{abs} = 1.1$ msec. The right-hand side is the blow-up of the solutions in a given period (not delay τ) to clearly illustrate the patterns of solutions.

for $t \in [s_2, s_2 + d_{abs}]$, where d_{abs} is the length of this period. The solution $x_{abs}(t) = V_r e^{-\beta(t-s_2)}$ is the same as the function η, which describes the form of the spike and spike afterpotential in the spike response model (SRM) when mapping the integrate-and-fire model to the SRM (Gerstner & Kistler, 2002). The absolute refractoriness allows the membrane potential to decay back from the hyperpolarization (afterpotential) to the resting potential even if feedback is delivered during this period.

In the periodic regime such as $I_s = 0.38\ \mu$A, we observe multiple coexisting attracting periodic solutions shown in Figure 3, with parameters $\tau = 116$ msec, $\beta = 0.08$, $c = 10$ mV, $a = 0.6$, $s_1 - t_f = 0.60$ msec, $s_2 - s_1 = 2.7$ msec, $\vartheta_1 = 1.2$ mV, $V_r = -1.1$ mV, and $d_{abs} = 1.1$ msec. Trajectories are output in six delay intervals after 50τ of transients. The right-hand side is the blow-up of the solutions in a given period (not delay τ) to clearly illustrate the patterns of solutions.

Ignoring the action potential and focusing on the small oscillatory part of these solutions, we found that there exist only two shapes, denoted by w and v, respectively. Because all solutions are composed of w and v, we can describe patterns in terms of the number and order where w and v appear within one period. Therefore, Figure 3 has three different patterns denoted by 3w8v, 1w2v2w6v, and 1w3v1w3v1w2v, respectively. Figure 4 lists three other patterns: 3w2v, 4w1v2w3v, and all v. These numerical observations clearly show the capacity of the LIF model for generating a large number of attracting periodic solutions.

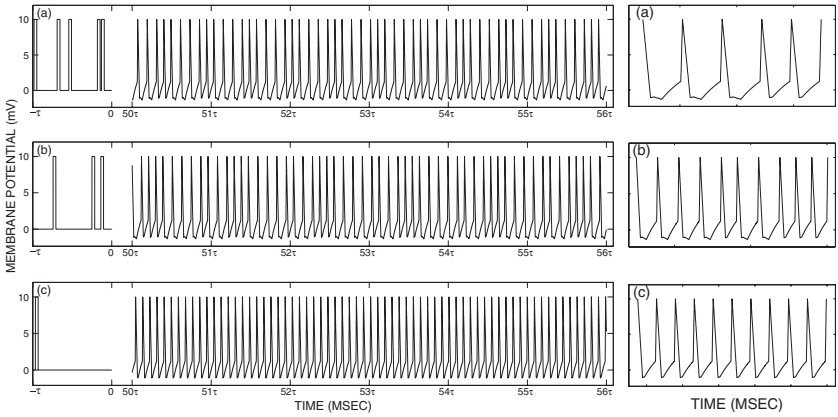

Figure 4: Three other asymptotically stable periodic patterns (3w2v, 4w1v2w3v and all v) generated by the LIF model given by equation 2.2 with the signal function $F_1(x)$ for $I_s = 0.38\ \mu$A and other parameters identical to those used in Figure 3. The right-hand side is the blow-up of the solutions in a given period (not delay τ) to clearly illustrate the patterns of solutions.

The advantage of the LIF model is that the equation can be analytically integrated, and such a dynamic system exhibits multistability in the periodic regime. Two important biological features of a single neuron are incorporated in the LIF model: the firing and absolute refractory period. The firing determines the possible timing T_ϑ of the corresponding feedback, and the absolute refractoriness determines whether such a feedback has impact on the excitatory neuron. If a feedback arrives at time s_3 during the absolute refractory period ($s_3 \in [s_2, s_2 + d_{abs})$), then the feedback affects the membrane potential of the excitatory neuron in only a small time interval, that is, the effective timing is of the duration $T_\vartheta - (s_2 + d_{abs} - s_3)$.

In contrast to results of the work of Foss et al. (1996), in the excitable regime and using various signal functions F including the one used in the work of Foss et al., spikes in an initial function for the LIF model cannot propagate in the subsequent delay intervals, and spike train patterns cannot be generated. The reason is that another important biological function of a single neuron, inhibitory rebound, is not captured by the LIF model. The quadratic integrate-and-fire model, incorporating a rebound equation, naturally solves this problem.

3.5 Quadratic Integrate-and-Fire Model. The quadratic integrate-and-fire model (QIF) was proposed in Feng (2001), Hansel and Mato (2001), and Latham et al. (2000):

$$\tau \frac{dx}{dt} = a_0(x - x_{rest})(x - x_c) + RI(t), \tag{3.5}$$

where x_{rest} is the resting membrane potential, a_0 and R are positive constants, and $x_c > x_{rest}$. When there is no external stimulus ($I(t) = 0$) and the initial condition $x(t) < x_c$, the membrane potential converges to the resting membrane potential x_{rest}. For $x(t) > x_c$, the membrane potential increases so that an action potential is triggered. The parameter x_c can therefore be interpreted as the critical potential for firing. From a biophysical point of view, x_c can be considered as a reversal potential due to the different ion concentrations between the interior of cell membrane and its surrounding liquid. In the QIF model, the relationship between a weak stimulus and the equilibrium of the membrane potential is a quadratic function.

One of the motivations for us to introduce the QIF model is to have a similar equation for the inhibitory rebound mechanism; another reason is to use the QIF instead of the LIF model is the capability of a QIF model to generate a large number of stable periodic patterns. In particular, we have used both LIF and QIF models for intensive simulations, and our simulations show that in the excitable region, both LIF and QIF models with an inhibitory rebound mechanism (described below) can generate similar results. However, in the periodic region, the QIF model can generate much more stable patterns than the LIF model. Furthermore, it is much easier to choose relevant parameter values to generate stable patterns by the QIF model, and the generated patterns are more distinguishable.

3.6 Inhibitory Rebound Spike. When an inhibitory input is imposed on a group of neurons for a short period of time and is then removed, some neurons respond with one or more inhibitory rebound spikes. The rebound occurs at the rebound time t_b, when the inhibitory input makes the membrane potential less than the so-called rebound threshold ϑ_2 and when the input is switched off so that $I(t_b^-) < 0$ and $0 \le I(t_b) < I_{\max}$, where $I_{\max}$ is the maximum value of an input that cannot make a neuron fire.

The QIF model alone, does not give inhibitory rebound spikes that seem to be a very important factor to permit the spike propagation in the excitable regime of recurrent inhibitory loops. To provide this inhibitory rebound mechanism, we need to introduce the following rebound equation,

$$\tau \frac{dx}{dt} = a_0(x - x_I)(x - x_c) + RI(t), \tag{3.6}$$

where $x_c > x_I$, x_I is the critical reversal potential of inhibitory rebound and x_c is the critical reversal potential of the firing introduced above. The rebound equation describes the dynamical behavior of the neuron from the rebound time t_b to the next spiking time. After the inhibitory input is switched off, if $x < x_I$ and if $x_I < \vartheta_1$, then the membrane potential $x(t)$ increases and finally approaches its equilibrium x_I when $I(t) = 0$, or reaches higher potential than x_I when $I(t) > 0$. If $x_I > \vartheta_1$ (the firing threshold) and

when the membrane potential reaches its firing threshold ϑ_1, the neuron fires and creates an action potential.

We can now formulate our rules that govern the evolution of the neuron potential for recurrent inhibitory loops. Let $x_{rest} = 0$. Then we have

$$x'(t) = \beta(x - \mu)(x - \gamma) - F(x(t - \tau)) + I_s, \tag{3.7}$$

where

$$\mu = \begin{cases} x_I & \text{if } x(t) \le \vartheta_2 \text{ and the inhibitory input is switched off} \\ x_{rest} = 0 & \text{otherwise,} \end{cases} \tag{3.8}$$

where β is a positive constant, $\vartheta_2 < 0$ is the rebound threshold, $x_I > \vartheta_1$ is the reversal potential of inhibitory rebound, and γ is the reversal potential of the firing. After the membrane potential reaches the firing threshold ϑ_1 at $t = t_f$, the potential time course is given by

$$x(t) = x_f(t), \qquad t \in [t_f, s_2]$$
$$x(t) = x_{abs}(t), \qquad t \in [s_2, s_2 + d_{abs}],$$

where $x_{abs}(t)$ is given by

$$\frac{dx_{abs}(t)}{dt} = \beta(x_{abs} - x_{rest})(x_{abs} - \gamma), \quad t \in [s_2, s_2 + d_{abs}], \tag{3.9}$$

with d_{abs} being the length of the absolute refractory period. Consequently, the rebound mechanism, the firing mechanism, and the absolute refractory period as intrinsic properties of a neuron are all incorporated into the QIF model.

Figure 5 shows three spike patterns (left) in the excitable regime $I_s = 0$ generated by the quadratic integrate-and-fire model, in comparison with the Hodgkin-Huxley model (right). For the QIF model, parameters are $\tau = 116$ msec, $\beta = 0.08$, $c = 10$ mV, $a = 0.9$, $s_1 - t_f = 0.60$ msec, $s_2 - s_1 = 2.7$ msec, $\vartheta_1 = 1.2$ mV, $V_r = -1.1$ mV, $\vartheta_2 = -0.8$ mV, $x_I = 2.5$, $\gamma = 3.0$, and $d_{abs} = 1.1$ msec. We note that solutions of the QIF model are very similar to those of the HH model. If spikes in an initial function ϕ are sufficiently separated, spikes will propagate and finally form stable periodic solutions as shown in Figures 5a and 5b. In such cases, different initial functions give rise to different solutions. If spikes in an initial function ϕ are too close, as in Figure 5c, spikes will eventually merge. There are no coexisting periodic attractors in the excitable regime. We point out that the rebound mechanism enables IPSP to bring the system state across the firing threshold separatrix,

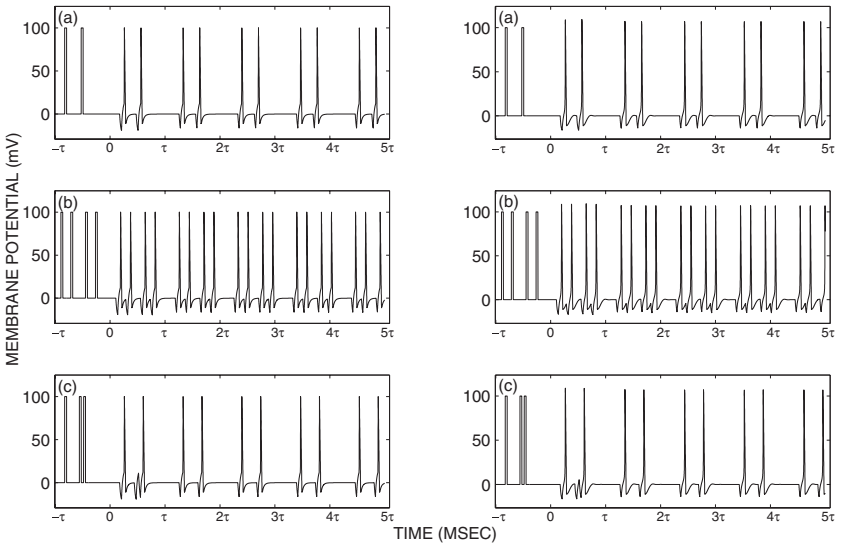

Figure 5: Three spike train patterns generated by the QIF model (left), in comparison with the Hodgkin-Huxley model (right) in the excitable regime $I_s = 0$. For the QIF model, parameters are $\tau = 116$ msec, $\beta = 0.08$, $c = 10$ mV, $a = 0.9$, $s_1 - t_f = 0.60$ msec, $s_2 - s_1 = 2.7$ msec, $\vartheta_1 = 1.2$ mV, $V_r = -1.1$ mV, $\vartheta_2 = -0.8$ mV, $x_I = 2.5$, $\gamma = 3.0$, and $d_{abs} = 1.1$ msec. In order to compare with the HH model, values of the QIF model are amplified 10 times. If spikes in an initial function are sufficiently separated (a, b), spikes will propagate without merging. If spikes are too close (c), spikes will merge.

following the release of an inhibition so that spikes in initial functions can propagate in future time.

Figure 6 shows, in the periodic regime $I_s = 0.38$ μA, five coexisting attracting periodic solutions generated by the QIF model with parameters $\tau = 116$ msec, $\beta = 0.08$, $c = 10$ mV, $a = 0.9$, $s_1 - t_f = 0.60$ msec, $s_2 - s_1 = 2.7$ msec, $\vartheta_1 = 1.2$ mV, $V_r = -1.1$ mV, $\vartheta_2 = -0.8$ mV, $x_I = 2.5$, $\gamma = 3.0$, and $d_{abs} = 1.1$ msec. After 50τ of transients, the periodic solutions are output in six delay intervals. The number of attractive periodic solutions composed of two w oscillations and nine v oscillations within one period is 5, and this is not a coincidence. It is equal to the number of different ways to arrange two w's and nine v's in a ring: $\frac{\binom{11}{2}\binom{9}{9}}{11} = 5$, and all possible arrangements of two w's and nine v's in a ring are

$$\left\{ \begin{array}{l} \text{wwvvvvvvvvvv, wvwvvvvvvvvv, wvvwvvvvvvvv,} \\ \text{wvvvwvvvvvvv, wvvvvwvvvvvv} \end{array} \right\}.$$

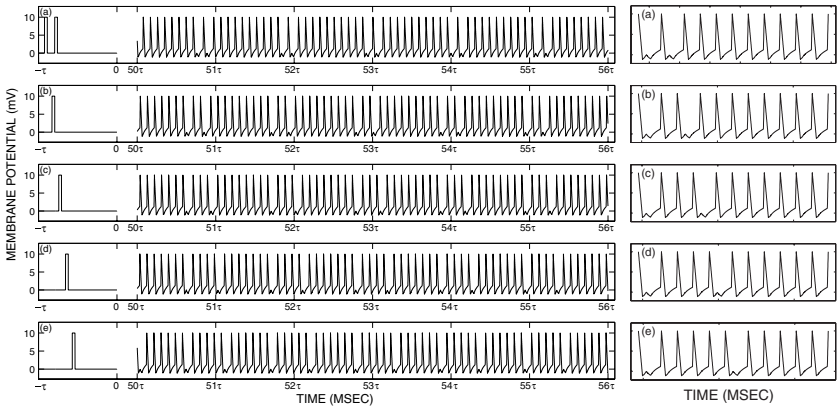

Figure 6: Five coexisting attracting periodic solutions of patterns: 2w9v, 1w1v1w8v, 1w2v1w7v, 1w3v1w6v, and 1w4v1w5v, generated by the QIF model in the periodic regime $I_s = 0.38\ \mu$A. Parameters are the same as those used in Figure 5. The right-hand side is the blow-up of the solutions in a given period (not delay τ) to clearly illustrate the patterns of solutions.

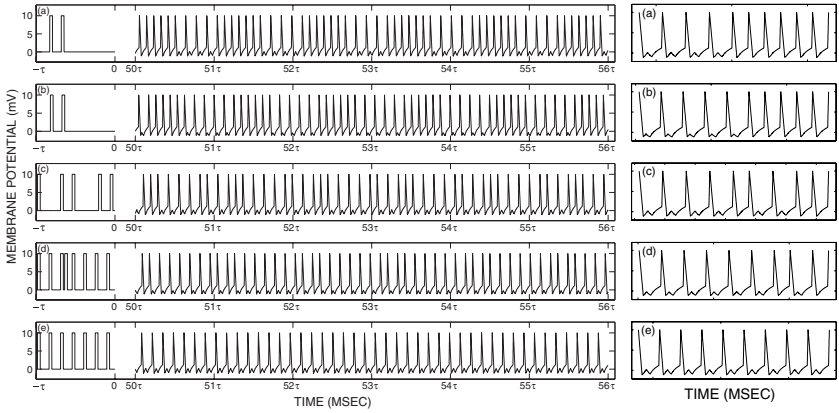

Figure 7: Five other patterns generated by the QIF model in the periodic regime $I_s = 0.38\ \mu$A. Parameters are identical to those in Figure 6. (a) Pattern 4w6v. (b) Pattern 5w5v. (c) Pattern 4w1v2w2v. (d) Pattern 6w1v1w1v. (e) Pattern wwwwwwwww. The right-hand side is the blow-up of the solutions in a given period (not delay τ) to clearly illustrate the patterns of solutions.

Figure 7 displays five other patterns: 4w6v, 5w5v, 4w1v2w2v, 6w1v1w1v, and wwwwwwwww.

Similar to the linear integrate-and-fire model, equation 3.7 can be integrated analytically. Let $I = I_s - F(x(t-\tau))$. In the intervals where I is a

Table 1: Number of Stable Patterns and Number of Distinct Periods When $\tau = nT$.

τ	Number of Patterns	Number of Periods	τ	Number of Patterns	Number of Periods
T	1	1	$5T$	4	3
$2T$	2	2	$6T$	6	4
$3T$	2	2	$7T$	8	4
$4T$	3	3	$8T$	13	5

constant, equation 3.7 can be written in the form

$$\frac{dx}{dt} = \beta(x - \lambda_1)(x - \lambda_2), \tag{3.10}$$

where

$$\lambda_1 = \frac{\mu + \gamma}{2} + \sqrt{\left(\frac{\mu - \gamma}{2}\right)^2 - \frac{I}{\beta}} \quad \text{and} \quad \lambda_2 = \frac{\mu + \gamma}{2} - \sqrt{\left(\frac{\mu - \gamma}{2}\right)^2 - \frac{I}{\beta}}.$$

The solution of the above equation is given by

$$x(t) = \begin{cases} \frac{\mu+\gamma}{2} + \frac{x(t_0) - \frac{\mu+\gamma}{2}}{1 - \beta(x(t_0) - \frac{\mu+\gamma}{2})(t - t_0)} & \text{if } (\mu - \gamma)^2 = \frac{4I}{\beta}; \\ \lambda_2 + \frac{(x(t_0) - \lambda_2)(\lambda_1 - \lambda_2)}{x(t_0) - \lambda_2 - (x(t_0) - \lambda_1)e^{\beta(\lambda_1 - \lambda_2)(t - t_0)}} & \text{if } (\mu - \gamma)^2 > \frac{4I}{\beta}, \end{cases} \tag{3.11}$$

where t_0 is an initial time. A similar but slightly more complicated formula can be derived if $(\mu - \gamma)^2 < \frac{4I}{\beta}$. Therefore, the trajectory for a given initial function ϕ can be analytically obtained. However, for most initial functions, it seems that trajectories exhibit quite exotic transient behaviors before they eventually become periodic.

Using the above analytical expression for solutions of the QIF model, we can calculate the number of stable periodic patterns and the number of distinct periods of stable periodic patterns, listed in Table 1 when $\tau = nT$, n is an integer from 1 to 8, and T is the intrinsic spiking period.

We explain how Table 1 is obtained at the end of this section. We point out that when $\tau \neq nT$, the results become more complicated due to two different types of W oscillation coexisting in one stable pattern and due to the transition from one subset of stable patterns to another at certain critical values of the time delay τ. We defer detailed discussions to future work but list in Tables 2, 3, and 4 some illustrative examples when $\tau \in (T, 2T)$, $\tau \in (2T, 3T)$, and $\tau \in (3T, 4T)$. In particular, in the region $(T, 2T)$, multistability occurs only in the subinterval $\tau \in (T + 0.5488T, T + 0.5552T]$.

Table 2: Number of Stable Patterns and Number of Distinct Periods When $\tau \in (T, 2T)$.

τ	Number of Patterns	Number of Periods
$(T, T + 0.1815T]$	1	1
$(T + 0.1815T, T + 0.3890T]$	1	1
$(T + 0.3890T, T + 0.5488T]$	1	1
$(T + 0.5488T, T + 0.5552T]$	2	2
$(T + 0.5552T, T + 0.6329T]$	1	1
$(T + 0.6329T, 2T)$	1	1

Table 3: Number of Stable Patterns and Number of Distinct Periods When $\tau \in (2T, 3T)$.

τ	Number of Patterns	Number of Periods
$(2T, 2T + 0.1815T]$	2	2
$(2T + 0.1815T, 2T + 0.3890T]$	2	2
$(2T + 0.3890T, 2T + 0.5488T]$	2	2
$(2T + 0.5488T, 2T + 0.5552T]$	4	3
$(2T + 0.5552T, 2T + 0.6329T]$	3	2
$(2T + 0.6329T, 2T + 0.7586T]$	2	2
$(2T + 0.7586T, 2T + 0.8486T]$	1	1
$(2T + 0.8486T, 2T + 0.8767T]$	2	2
$(2T + 0.8767T, 2T + 0.9290T]$	2	2
$(2T + 0.9290T, 3T)$	1	1

Table 4: Number of Stable Patterns and Number of Distinct Periods When $\tau \in (3T, 4T)$.

τ	Number of Patterns	Number of Periods
$(3T, 3T + 0.1815T]$	2	2
$(3T + 0.1815T, 3T + 0.3890T]$	2	2
$(3T + 0.3890T, 3T + 0.5488T]$	2	2
$(3T + 0.5488T, 3T + 0.5552T]$	5	3
$(3T + 0.5552T, 3T + 0.6329T]$	4	2
$(3T + 0.6329T, 3T + 0.8486T]$	3	3
$(3T + 0.8486T, 3T + 0.8767T]$	6	4
$(3T + 0.8767T, 3T + 0.9290T]$	4	4
$(3T + 0.9290T, 4T)$	2	2

In the region $(2T, 3T)$, multistability cannot occur in the intervals $\tau \in (2T + 0.7586T, 2T + 0.8486T] \cup (2T + 0.9290T, 3T)$. And in region $(3T, 4T)$, multistability occurs everywhere.

3.7 Phase Resetting Properties. The effect of the IPSP in the QIF model can be summarized by the phase reset curve (PRC). PRC describes the phase shift related to the phase at which the IPSP arrives in the neuron's spike

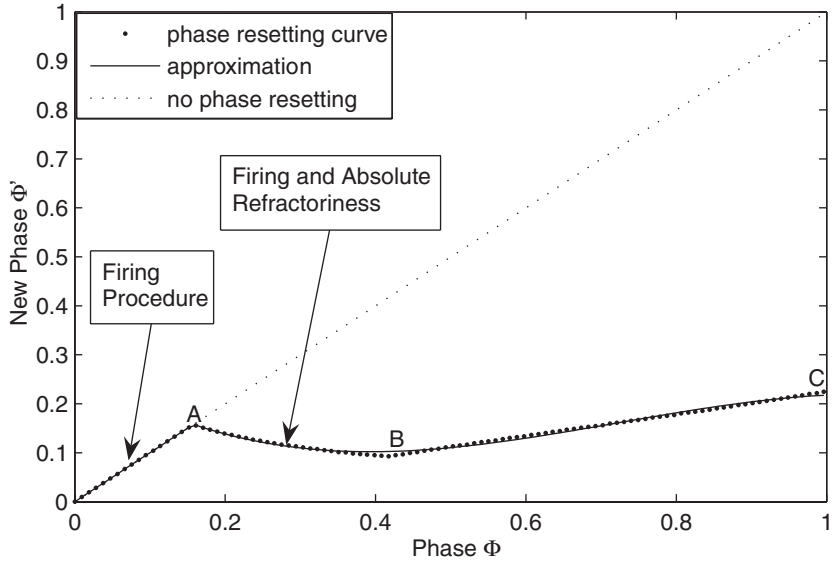

Figure 8: The phase-resetting curve (point curve), its approximation (solid curve) of the QIF model, and the dotted line of no phase resetting ($\Phi' = \Phi$).

time. The phase Φ at which the IPSP arrives is

$$\Phi = \frac{t_p - t_f}{T}, \tag{3.12}$$

where t_p is the time that the IPSP is delivered, t_f is the firing time of the last spike, and T is the intrinsic spiking period (Foss & Milton, 2000). Following the arrival of the IPSP, the phase has been reset by an amount Δ called the *phase reset*, which is defined by

$$\Delta = 1 - \frac{t_1 - t_f}{T}, \tag{3.13}$$

where t_1 is the firing time of the next spike. The new phase Φ' is easily calculated by

$$\Phi' = \Phi + \Delta. \tag{3.14}$$

Figure 8 shows the phase-resetting curve (point curve) of the QIF model, a plot of the new phase Φ' versus the original phase Φ, and the approximation (solid curve) and the dotted line of no phase resetting ($\Phi' = \Phi$) when $T = 10.54$ msec and other parameters are identical to those used in

Figure 7. From the original point (0,0) to point A, the new phase is equal to the original phase ($\Phi' = \Phi$) because the IPSP does not affect the membrane potential during the period of firing. From point A to B, the new phase (Φ') decreases as the original phase (Φ) increases because the absolute refractoriness reduces the effective timing of the feedback that affects the excitatory neuron. After the absolute refractoriness, from point B to point C, the full IPSP affects the excitatory neuron, and the new phase increases. The approximation was obtained by a least-square fitting to the phase-reset curve that gives rise to

$$\Delta(\Phi) = \begin{cases} 0 & \text{if } \Phi < 0.1575 \\ a_3\Phi^3 + a_2\Phi^2 + a_1\Phi + a_0 & \text{otherwise,} \end{cases} \tag{3.15}$$

where $a_3 = -0.8287$, $a_2 = 1.7939$, $a_1 = -2.0261$, and $a_0 = 0.27859$, and the root mean square (rms) error is 0.003577.

Each time the neuron fires a spike, an IPSP or feedback is delivered at time τ later. We denote Φ_n as the phase of the nth IPSP due to a spike S_n. The phase Φ_n is determined by

$$\Phi_n = \frac{\tau}{T} + \sum_{i=1}^{k} \Delta(\Phi_{n-i}) - N, \tag{3.16}$$

where k is the number of other IPSPs in the interval between Φ_n and the spike S_n, and N is the number of spikes in this interval (see details in Foss & Milton, 2000). We introduce a new variable Ψ, defined by

$$\Psi = \Phi + N. \tag{3.17}$$

Then equation 3.16 can be rewritten as

$$\Psi_n = \frac{\tau}{T} + \sum_{i=1}^{k} \Delta(\Phi_{n-i}) = F(\Psi_{n-1}, \Psi_{n-1}, ..., \Psi_{n-k}), \tag{3.18}$$

where $\Phi_i = \Psi_i \bmod 1$. When a pattern is asymptotically approached, Ψ approaches one of its fixed points Ψ^*, which are the solutions of the equation

$$f(\Psi) = g(\Psi), \tag{3.19}$$

where

$$f(\Psi) = \Psi - \frac{\tau}{T}, \qquad \text{and} \qquad g(\Psi) = k\Delta(\Psi),$$

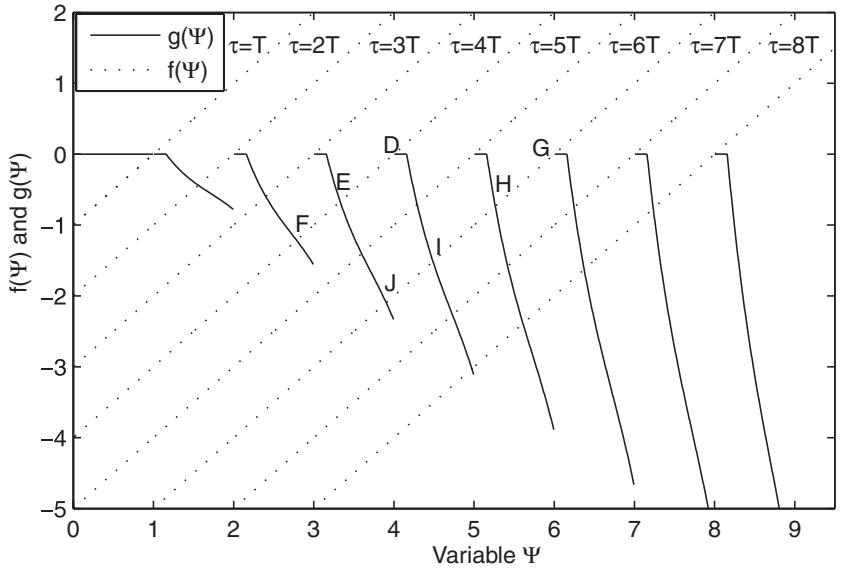

Figure 9: Critical points of equation 3.19 for different values of the time delay τ. Function $f(\Psi)$ is the dotted line, and function $g(\Psi)$ is the solid curve. Critical points for equation 3.19 are 1 for $\tau = T$, 2 for $\tau = 2T$, 2 for $\tau = 3T$, 3 for $\tau = 4T$, 3 for $\tau = 5T$, 4 for $\tau = 6T$, 4 for $\tau = 7T$, and 5 for $\tau = 8T$. We label three critical points (D, E, F) for $\tau = 4T$ and four points (G, H, I, J) for $\tau = 6T$.

k is the nearest integer that Ψ is rounded down to. Foss and Milton (2000) suggested that the condition for these solutions to be stable is that the slope S^* of $\Delta(\Phi)$ evaluated at the fixed point satisfies $-1 < S^* < k^{-1}$.

Figure 9 shows the plot of $f(\Psi)$ and $g(\Psi)$ as functions of Ψ, where the approximation 3.15 is used. Critical points for equation 3.19 are 1 for $\tau = T$, 2 for $\tau = 2T$, 2 for $\tau = 3T$, 3 for $\tau = 4T$, 3 for $\tau = 5T$, 4 for $\tau = 6T$, 4 for $\tau = 7T$, and 5 for $\tau = 8T$. Having only one fixed point when $\tau < T$ implies that multistability seems unlikely to arise in such a case. These numbers of critical points coincide exactly with the numbers of distinct periods of stable patterns listed in Table 1. This coincidence suggests that each critical point represents a subset of stable periodic solutions, in which different periodic solutions have the same period rather than just one stable pattern. All periodic solutions in such a subset have the same configuration; they are composed of the same number of w oscillations and the same number of v oscillations within one period, but the orders where w and v appear may be different.

Knowing the configuration of each subset, we are able to calculate the number of periodic solutions in the subset and predict the patterns of these

periodic solutions. To be more precise, we denote the set of all periodic solutions of $\tau = nT$ as Ω_{nT} and a subset composed of m w oscillations and h v oscillations within one period as $\Omega_{m,h}$, where $m + h \leq n$. When $\tau = 4T$, $\Omega_{4T} = \Omega_{1,0} \cup \Omega_{0,1} \cup \Omega_{3,1}$. There is only one periodic solution 1w in $\Omega_{1,0}$ and one periodic solution 1v in $\Omega_{0,1}$. The number of periodic solutions in $\Omega_{3,1}$ is $\frac{\binom{4}{3}\binom{3}{3}}{4} = 1$ and $\Omega_{3,1} = \{3w1v\}$. Hence, $\Omega_{4T} = \{1w, 1v, 3w1v\}$. When $\tau = 6T$, $\Omega_{6T} = \Omega_{1,0} \cup \Omega_{0,1} \cup \Omega_{1,1} \cup \Omega_{3,3}$. For the subset $\Omega_{1,1}$, the number of periodic solutions is $\frac{\binom{2}{1}\binom{1}{1}}{2} = 1$, and the periodic solution is 1w1v1w1v1w1v. For the subset $\Omega_{3,3}$, the number of periodic solutions composed of three w's and three v's is $\frac{\binom{6}{3}\binom{3}{3}-2}{6} = 3$ because two possible arrangements for pattern 1w1v (actually 1w1v1w1v1w1v has been counted in the subset $\Omega_{1,1}$) must be deducted; hence, $\Omega_{3,3} = \{3w3v, 2w2v1w1v, 2w1v1w2v\}$. Using this approach to calculate the number of periodic solutions in a subset, we can calculate the number of periodic solutions for $\tau = 8T$ as $1 + 1 + \frac{\binom{8}{3}\binom{5}{5}}{8} + \frac{\binom{7}{5}\binom{2}{2}}{7} + \frac{\binom{7}{6}\binom{1}{1}}{7} = 13$.

From Table 1, we conclude that both the number of stable patterns and the number of distinct periods of stable patterns increase as n increases when $\tau = nT$ and n is an integer. However, when $\tau = nT + t_0$ and $0 < t_0 < T$, the stable periodic patterns become more complicated because in addition to a v oscillation, two types of w oscillation may coexist in one pattern in a certain region (a neighborhood around $t_0 = 0.6T$), which are denoted by W_1 (down and up) and W_2 (up, down, and up) (the notation is introduced to demonstrate the shape of oscillations after the absolute refractory period (from time $s_2 + d_{abs}$ to the next firing time t_f)). The coexistence of two types of w oscillations significantly increases the number of stable patterns, though it does not increase the number of distinct periods of stable patterns. This suggests that as far as multistability is concerned, we need to pay more attention to the distinct periods of stable patterns.

Compared with the linear integrate-and-fire model (LIF), the neural intrinsic inhibitory rebound mechanism is incorporated into the quadratic integrate-and-fire model, and it allows spikes in an initial function to propagate in subsequent delay intervals in the excitable regime. In the periodic regime, both the firing and absolute refractory period are the key for simple phenomenological spiking neuron models to generate a large number of coexisting stable patterns. The firing determines the possible timing of the feedback, and the absolute refractory period determines whether the feedback has an impact on the excitatory neuron. The coexistence of three different oscillations W_1, W_2, and v significantly increases the number of stable periodic patterns but does not affect the number of distinct periods of stable periodic patterns. The number of critical points of the phase-resetting map coincides exactly with the number of the distinct periods of stable patterns we analytically calculated. Properties of the multiple

distinct periods of stable patterns seem to be an important issue in the study of multistability.

Perhaps it is worth mentioning that the quadratic integrate-and-fire neuron is closely related to the so-called θ-neuron, a type of canonical type I neuron (Latham et al., 2000), given by

$$\frac{d\varphi}{dt} = (1 - \cos\varphi) + \Delta I(1 + \cos\varphi), \tag{3.20}$$

where $\Delta I = I - I_\theta$ and I_θ denotes the minimal current necessary for repetitive firing of the model.

3.8 More on the Number of Periodic Patterns. We now briefly explain how the results in Table 1 were obtained. The key is to determine what kind of subsets $\Omega_{m,h}$ (composed of m W oscillations and h V oscillations) can exist when $\tau = nT$ for a given integer n. Once this is done, we use the approach described above to calculate the number of stable patterns.

First, we note that $\Omega_{0,1} \subseteq \Omega_{nT}$ for any positive integer n, that is, periodic pattern 1V, can always be generated. Second, we remark that $\Omega_{1,0} \subseteq \Omega_{nT}$ when $n \geq 2$, that is, periodic pattern 1W can always be generated when $n \geq 2$. The existence of the other subset $\Omega_{m,h}$ with $m, h \geq 1$ depends on variables T, T_{FR}, and T_ϑ determined by the QIF model, where T is the intrinsic spiking period, T_ϑ is the possible feedback timing, and T_{FR} is the sum of the firing period and absolute refractory period. For a periodic pattern in $\Omega_{m,h}$, all W oscillations have the same shape, characterized by $(t_{up}, T_\vartheta, t_{1\vartheta})$(up, down, up). Here the notation means that after the absolute refractoriness, the membrane potential first increases for t_{up} msec, then decreases for T_ϑ msec due to a feedback, and finally increases to the firing threshold ϑ_1 for $t_{1\vartheta}$ msec. The condition of the existence of such periodic patterns is

$$0 < t_{up} = \frac{(n + 1 - m - h)T - [T_{FR} + (m - 1)(T_\vartheta + t_{1\vartheta} - T + T_{FR})]}{m} \leq T_c$$

for a parameter T_c determined by the QIF model. We are able to use the relationship among T, T_{FR}, and T_ϑ in our simulations to determine what kind of subset $\Omega_{m,h}$ can exist for a given n. For example, when $\tau = 4T$, the above condition for the subset $\Omega_{3,1}$ is satisfied. Therefore, $\Omega_{4T} = \{1\text{w}, 1\text{v}, 3\text{w}1\text{v}\}$.

4 Discussion

We have focused on the asymptotic behaviors of the excitation neuron in a recurrent inhibitory loop, and our emphasis is on the capability of such a single loop to generate multiple stable patterns. Although the well-known Hodgkin-Huxley model has been previously used to address this

multistability issue in Foss et al. (1996), such a dynamic system of four degrees of freedom is difficult to visualize and analyze. Our study shows that the key to generating a large number of coexisting stable patterns in simple phenomenological models is the incorporation of firing and the absolute refractory period. The effect of both time delay and effective timing of the feedback on the excitatory neuron determines the type of the multistability. The firing procedure determines the possible timing of the feedback that affects the excitatory neuron. The absolute refractoriness increases the complexity of stable periodic patterns by changing the effective timing of the feedback on the excitatory neuron.

Our simulation results show that a recurrent inhibitory loop based on the simple phenomenological spiking neuron models exhibits coexisting multiple attracting periodic solutions in the periodic regime. These solutions can be categorized in terms of the symbols w and v, and the corresponding periodic patterns can be predicted by considering different ways of arranging w and v in a ring.

The inhibitory rebound mechanism seems to play a very important role in spike propagation in the excitable regime for recurrent inhibitory loops. The quadratic integrate-and-fire model (QIF) captures very well this inhibitory rebound period using the rebound equation.

The phase-resetting curve provides a powerful tool to study multistability in recurrent inhibitory loops based on simple phenomenological spiking neuron models. Our study shows that the number of fixed points of the phase-resetting map coincides with the number of distinct periods of stable patterns rather than the number of stable patterns when $\tau = nT$ and n is an integer. With the help of the configurational information corresponding to these critical points, we are able to calculate the number of the stable periodic patterns and predict these stable periodic patterns.

For the recurrent inhibitory loop discussed in this article, the effect of the inhibitory postsynaptic potential (IPSP) from the inhibitory neuron I to the excitatory neuron E is simplified as a delayed self-feedback of the membrane potential of the excitatory neuron E. Under this simplification, we need only to consider dynamical behaviors of the single excitatory neuron E, and hence the model equation takes the form of a scalar delay differential equation. However, a more realistic approach for such a two-neuron network must be based on the coupled differential equations,

$$\begin{cases} x'(t) = \beta(x-\mu)(x-\gamma) - F(y(t)) + I_s \\ y'(t) = \beta(y-\mu)(y-\gamma) + F(x(t-\tau)), \end{cases} \tag{4.21}$$

with the firing time t_{f_x} and t_{f_y}

$$\begin{cases} t_{f_x} : x(t) = \vartheta_1 \quad \text{and} \quad x'(t)|_{t=t_{f_x}} > 0 \\ t_{f_y} : y(t) = \vartheta_1 \quad \text{and} \quad y'(t)|_{t=t_{f_y}} > 0, \end{cases} \tag{4.22}$$

for the excitatory neuron and the inhibitory neuron, where $x(t)$ is the membrane potential of the excitatory neuron E, $y(t)$ is the membrane potential of the inhibitory neuron I, and $F(x)$ is the signal function. Detailed study of equations 4.21 remains a challenging task for the future.

Acknowledgments

This research was partially supported by Canada Research Chairs Program, by National Sciences and Engineering Research Council of Canada, and by Mathematics for Information Technology and Complex Systems. We thank the two reviewers whose comments led to a substantial improvement of our manuscript.

References

an der Heiden, U., & Mackey, M. C. (1982). The dynamics of production and destruction: Analytic insight into complex behaviour. *Math. Biol., 16*, 75–101.

Canavier, C., Baxter, D., Clark, J., & Byrne, J. (1994). Multiple modes of activity in a model neuron suggest a novel mechanism for the effects of neuromodulators. *J. Neurophysiol., 72*, 872–882.

Canavier, C., Butera, R., Dror, R., Baxter, D., Clark, J., & Byrne, J. (1999). Phase response characteristics of model neurons determine which patterns are expressed in a ring circuit model of gait generation. *Bio. Cybern., 77*, 367–380.

Chen, Y., & Wu, J. (1999). Minimal instability and unstable set of a phase-locked periodic orbit in a delayed neural network. *Phys. D, 134*, 185–199.

Chen, Y., & Wu, J. (2000). *Limiting profiles of periodic solutions of neural with synaptic delays*. Singapore: World Scientific.

Chen, Y., & Wu, J. (2001). Existence and attraction of a phase-locked oscillation in a delayed network of two neurons. *Differential Integral Equations, 14*, 1181–1236.

Chen, Y., & Wu, J. (2001b). Slowly oscillating periodic solutions for a delayed frustrated network of two neurons. *J. Math. Appl., 259*, 118–208.

Chen, Y., & Wu, J. (2001c). The asymptotic shapes of periodic solutions of a singular delay differential system. *J. Differential Equations, 169*, 614–632.

Chen, Y., Wu, J., & Krisztin, T. (2000). Connecting orbits from synchronous periodic solutions in phase-locked periodic solutions in a delay differential system. *J. Differential Equations, 163*, 130–173.

Feng, J. (2001). Is the integrate-and-fire model good enough: A review. *Neural Comput., 13*, 955–975.

Foss, J., Longtin, A., Mensour, B., & Milton, J. (1996). Multistability and delayed recurrent loops. *Phys. Rev. Lett., 76*, 708–711.

Foss, J., & Milton, J. (2000). Multistability in recurrent neural loops arising from delay. *J. Neurophysiol., 84*(2), 975–985.

Foss, J., Moss, F., & Milton, J. (1997). Noise, multistability, and delayed recurrent loops. *Phys. Rev. E, 55*, 4536–4543.

Gerstner, W., & Kistler, W. M. (2002). *Spiking neuron models, single neurons, populations, plasticity*. Cambridge: Cambridge University Press.

Hansel, D., & Mato, G. (2001). Existence and stability of persistent states in large neuronal networks. *Phys. Rev. Lett., 86*, 4175–4178.

Hopfield, J. J. (1982). Neural networks and physical systems with emergent collective computational abilities. *Proc. Natl. Acad. Sci., 79*, 2554–2558.

Hopfield, J. J. (1984). Neurons with grades response have collective computational properties like those of two-state neurons. *Proc. Natl. Acad. Sci., 81*, 3088–3092.

Hoppensteadt, F., & Izhikevich, E. (1997). *Weakly connected neural networks*. New York: Springer-Verlag.

Ikeda, K., & Matsumoto, K. (1987). High-dimensional chaotic behavior in systems with time-delayed feedback. *Physica D, 29*, 223–235.

Latham, P. E., Richmond, B. J., Nelson, P. G., & Nirenberg, S. (2000). Intrinsic dynamics in neuronal networks. I. theory. *J. Neurophysiol., 83*, 808–827.

Losson, J. (1991). *Multistability and probabilistic properties of delay differential equations*. Unpublished master's thesis, McGill University.

Losson, J., Mackey, M. C., & Longtin, A. (1993). Solution multistability in first-order nonlinear differential delay equations. *Chaos, 3*, 167–176.

Mackey, M. C., & Glass, L. (1997). Oscillation and chaos in physiological control systems. *Science, 197*, 287–289.

Mackey, M. C., & an der Heiden, U. (1984). The dynamics of recurrent inhibition. *Math. Biol., 19*, 211–225.

Mackey, M. C., & Milton, J. G. (1987). Dynamical diseases. *Ann. New York Acad. Sci., 504*, 16–32.

Milton, J. (2000). Epilepsy: Multistability in a dynamic disease. In J. Walleczed (Ed.), *Self-organized biological dynamics and nonlinear control* (pp. 374–386). Cambridge: Cambridge University Press.

Morita, M. (1993). Associative memory with non-monotone dynamics. *Neural Networks, 6*, 115–123.

Schindler, K., Bernasconi, C., Stoop, R., Goodman, P., & Douglas, R. (1997). Chaotic spike patterns evoked by periodic inhibition of rat cortical neurons. *Z. Naturforsch, 25a*, 509–512.

Traub, R. D., & Miles, R. (1991). *Neuronal networks of the hippocampus*. Cambridge: Cambridge University Press.

Received February 5, 2006; accepted November 29, 2006.